PCCP

ROYAL SOCIETY OF CHEMISTRY

PAPER

Published on 25 June 2026

Cite this: DOI: 10.1039/d6cp01899h

Activation of methane by the tantalum trioxide anion, TaO_3^-

Tatsuya Chiba, †[a] Turbasu Sengupta, †[b] Shiying Wang, [a] Martin Tschurl, [c] Ulrich Heiz, [c] Shiv N. Khanna *[d] and Kit H. Bowen *[a]

Received 22nd May 2026,
Accepted 24th June 2026

DOI: 10.1039/d6cp01899h

rsc.li/pccp

To better utilize abundant supplies of methane, a catalyst is needed that can selectively activate it. Studies of the reactivity of methane with ions in the gas phase can provide insight into reaction mechanisms at specific catalytic sites. Recently, He *et al.* found, through mass spectrometric observations, that out of the 27 $[Ta_xO_y]^-$ species investigated, only $[TaO_3]^-$ formed an anion–methane complex, $[TaO_3CH_4]^-$ (Q. Li, Q.-Y. Liu, A. Zhao, and S.-G. He, Reactions between $Ta_xO_y^-$ (x = 1–5, y = 0–7) cluster anions and C_1–C_3 alkanes, *J. Chem. Phys.*, 2025, **163**, 054303). In the present study, where we employed a synergistic combination of anion photoelectron spectroscopy and DFT calculations, the $[TaO_3]^-$ isomer with a structure of O-Ta-O_2, in which the Ta atom is bonded to a terminal O atom and an η^1-superoxo $[O_2^-]$ ligand, was found to form two activation complexes with methane. The geometrical structures of these two activation complexes, in which one and two C–H bonds are cleaved respectively, were determined by comparing the experimental and computational spectra. This reports the first spectroscopic confirmation of C–H bond activation by tantalum oxide anions.

1. Introduction

While methane, which is the dominant component of natural gas, is an abundant C1 resource, it has been underutilized due to its strong C–H bond (438.990 ± 0.026 kJ mol^{-1})[1] and the cost of transporting gaseous methane. The unused methane at the oil extraction sites has been burned to CO_2 (the so-called flaring), partly because methane has a greenhouse effect that is 25 times greater than CO_2 on a mole basis.[2] The development of catalysts that enable on-site conversion of methane to valuable chemicals such as methanol and larger hydrocarbons would bring enormous economic and environmental benefits. These products are useful starting material for chemical industry and easy to transport.[3–6] However, since the C–H bonds of the desired products (402.44 ± 0.27 kJ mol^{-1} for methanol,[1] for example) are weaker than that of methane, the use of harsh conditions or highly reactive catalysts leads to a loss of selectivity. Due to its economic/environmental impact and the scientific challenges involved, the selective functionalization of methane has been called the "Holy Grail" of chemistry.[7]

Much research on the catalytic activities of bulk phase transition metal oxides towards methane has been carried out, this work usually having been motivated by industrial applications.[8] At the microscopic/atomistic level, however, the fundamental understanding of reaction mechanisms that might guide the design of catalysts has often come from gas-phase experiments, these involving studies where metal oxide ions were allowed to interact with methane molecules. The first two metal oxide ions shown to activate methane in the gas phase are OsO_n^+ (n = 0,1,2,4) by Beauchamp *et al.* in 1989[9] and FeO^+ by Schwarz *et al.* in 1990.[3] In both cases, the product cations were observed by Fourier transform ion cyclotron resonance (FT-ICR) spectrometry. In addition, catalytic activities of tantalum atomic/cluster cations[10–23] and tantalum-containing clusters[23–34] have also incited significant interest. These include the reactivities of $Ta_xO_y^+$ towards methane[19,23,27–30] as well as various hydrocarbons.[31–34] For example, among the metal dioxide cations of the Group V metals (MO_2^+, M = V, Nb, Ta), only TaO_2^+ activated methane to form $[Ta(O)(OH)(CH_3)]^+$, due to the strong Ta–C bond.[27] TaO_3^+ was also revealed to dehydrogenate methane and to release methylene, as well as to oxidize methane and to release methanol and formaldehyde.[28]

Comparing the reactivities of transition metal oxide cations and anions with a particular molecule provides deeper insights into the relevance of charge states in catalytic systems.

[a] Department of Chemistry, Johns Hopkins University, Baltimore, Maryland 21218, USA. E-mail: snkhanna@vcu.edu
[b] Department of Chemistry, School of Advanced Sciences, VIT-AP University, Beside AP Secretariat, Amaravati, Andhra Pradesh 522241, India
[c] TUM School of Natural Sciences and Catalysis Research Center, Technical University of Munich, 85748 Garching, Germany. E-mail: tschurl@tum.de
[d] Department of Physics, Virginia Commonwealth University, Richmond, Virginia 23284, USA. E-mail: kbowen@jhu.edu
† These authors contributed equally.

However, despite extensive investigations of cation reactions, the corresponding study of anion reactions has been limited. Castleman *et al.* examined the reactivities of $Nb_xO_y^-$ and $Ta_xO_y^-$, and showed that they are unreactive toward *n*-butane.[34] The first example of metal oxide cluster anions activating methane was $La_6O_{10}^-$, shown by He, Zheng, and co-workers in 2014.[35] Mass spectrometric observation of the reaction product anions, and determination of the $La_6O_{10}^-$ structure by anion photoelectron spectroscopy (aPES) combined with density functional theory (DFT) calculations showed that methane was activated at an oxygen-centered radical site.[35] He *et al.* showed in 2022 that $(MoO_3)_5O^-$ activates methane by the same mechanism.[36] In 2019, He, Zheng and co-workers showed that $RhVO_3^-$ activates methane and subsequently reacts with CO_2 to produce methanol, formaldehyde, and carbon monoxide at elevated reaction temperatures; this established the catalytic cycle of $CH_4 + CO_2 \rightarrow CH_3OH + CO$.[37] Using aPES and DFT calculations, they determined the geometrical structures of $RhVO_3^-$ and $[RhVO_3CH_4]^-$ anion complex as well as its reaction pathway. In 2025, He *et al.* examined the reactivities of 27 $Ta_xO_y^-$ (x = 1–5, y = 0–7) species with methane.[38] Out of these anions, they found, through mass spectrometric observations, that only TaO_3^- formed the anion–methane complex. The reaction rate of $[TaO_3CH_4]^-$ complex formation was determined to be $k = 3.2 \times 10^{-11}$ cm^3 s^{-1} molecule^{-1}. In their study of the isoelectronic anion, TaS_3^-, the high kinetic isotope effect, *i.e.*, 4.4, observed during the addition reaction of CH_4 *vs.* CD_4, indicated that TaS_3^- cleaves the C–H bond of methane.[39] Their DFT calculations predicted that TaS_3^- has a trigonal pyramidal structure and activates the C–H bond of methane through Lewis acid–base pairs (LABP) of $Ta^{\delta+}$–$S^{\delta-}$.[39] Based on this result, they predicted TaO_3^- to activate methane by the same mechanism.[38] While they also calculated the reaction pathway of the trigonal pyramidal TaO_3^- activating a methane, experimental confirmations of the geometrical structures of $[TaO_3CH_4]^-$ have not yet been achieved.

In this study, we produced $[TaO_3]^-$ by laser vaporization and allowed it to react with deuterated methane to form the $[TaO_3CD_4]^-$ anion complex, with the goal to provide experimental evidence for the C–H bond activation of methane by this compound. The anion photoelectron spectra of $[TaO_3]^-$ and $[TaO_3CD_4]^-$ revealed that $[TaO_3]^-$ activated methane. Combining these experimental spectra with DFT calculations identified a particular isomer of $[TaO_3]^-$, and showed that it formed two types of activation complexes with methane. Their geometrical structures, in which one and two C–H bonds of methane were cleaved respectively, were determined [see Fig. 6(d) and 7]. While there have been aPES studies of tantalum oxide cluster anions, such as $Ta_3O_3^-$,[40] TaO_n^- (n = 1–3),[41] and $Ta_3O_n^-$ (n = 1–8),[42] that provided information about their electronic structures, the present work provides the first example in which an anion complex, comprising a tantalum oxide anion and a reactant molecule, was investigated *via* the combination of aPES and theory. It showed the C–H bond activation by tantalum oxide anions for the first time by experiment.

2. Methods

2.1. Experimental methods

The experiments were conducted using an apparatus consisting of a laser vaporization ion source, a time-of-flight mass spectrometer, and an anion photoelectron spectrometer. The details of the apparatus are described elsewhere.[43] $[TaO_3]^-$ anion was produced by ablating a translating and rotating tantalum foil wrapped onto an aluminum rod with a second harmonic output of a Nd:YAG laser (532 nm, Continuum, Surelite II-10). Laser vaporization of the tantalum foil, that had an oxide layer on the metal surface, produced tantalum oxide anions without the need for an external source of oxygen. Subsequently, a gas mixture of CD_4/He (5%/95%, total pressure 40 psig ($\sim$380 kPa)) was pulsed from a pulse valve (Parker-Hannifin) over the laser-ablated tantalum foil, to make $[TaO_3]^-$ encounter the CD_4 molecule. The resultant anions were extracted to a Wiley-McLaren type time-of-flight mass spectrometer (TOF-MS). To record the anion photoelectron spectra (aPES), the anions of interest were mass-gated, decelerated, and photodetached by the second and third harmonic outputs of a Nd:YAG laser (532 nm and 355 nm, Continuum, Surelite I-20). The kinetic energy of the photodetached electrons (EKE) was recorded by a magnetic bottle electron energy analyzer. The electron binding energy (EBE) was obtained from EKE by the energy conservation relationship: $h\nu$ = EBE + EKE, where $h\nu$ is the photon energy of the laser. The photoelectron spectra were calibrated by the well-known transitions of Pb^- for the 532 nm aPES,[44,45] and Cu^- for the 355 nm aPES.[46] In this experiment, CD_4 was used instead of CH_4, to achieve an improved mass selectivity of aPES.

2.2. Computational methods

The global minima search of $[TaO_3]^-$ anion and related complexes are conducted using the Artificial Bee Colony (ABC) algorithm as implemented in ABCluster[47,48] package in combination with Gaussian16[49] for geometry optimization and energy evaluation. Two different density functional and basis set combinations, namely B3LYP/def2-SVP and PBE0/SDD, are employed in the minima searching process that encompassed more than 400 initial geometries generated by isomer module of ABCluster. Both approaches showed consistent results in identifying three isomers. For accurate evaluation of relative energy ordering and structure, the geometries of these three isomers are further optimized using B3LYP/def2-QZVPD level of theory. Spin multiplicity range of 1–5 is also examined during the optimization. All possible $[TaO_3(CH_4)]^-$ geometries were generated utilizing the geom module of ABCluster[47,48] in combination with Gaussian16.[49] For computational convenience, the deuterium atoms (D) were replaced with hydrogen atoms (H). During the search for the optimized geometries of $[TaO_3(CH_4)]^-$, the $[TaO_3]^-$ isomer geometry was kept fixed at the center, whereas the approach directions of CH_4 were varied as per ABC algorithm to obtain a substantial number of initial geometries. Subsequently, the same procedure as employed for $[TaO_3]^-$ was followed. Vibrational frequencies of optimized geometries are calculated to ensure that all the obtained

isomers are true minima without any imaginary frequencies. The simulated photoelectron spectra were obtained using generalized Koopmans approximation using Multiwfn[50,51] package, whereas a shift value of E_{HOMO} + VDE was utilized for each spectrum. A Gaussian broadening function with FWHM value of 0.4 eV was used to simulate the experimental aPES.

3. Results and discussion

3.1. Experimental results

Fig. 1 shows the recorded mass spectra. Laser vaporization of a tantalum foil with an oxide layer on the metal surface produced $[TaO_n]^-$ (n = 1–3) without backing gas. It also formed TaC_n^- (n = 1, 2) and $TaCD^-$, due to the carbon and deuterium atoms remaining on the metal surface after the previous repeated laser ablation with CD_4 gas. Pulsing CD_4/He gas mixture over the laser-ablated tantalum foil produced the $[TaO_3CD_4]^-$ anion complex as well as the dehydrogenated anions, $[TaO_3CD_n]^-$ (n = 0–3). Fig. 2 shows the anion photoelectron spectra of $[TaO_3]^-$ and $[TaO_3CD_n]^-$ (n = 0, 2, 4) recorded with 532 nm photons ($h\nu$ = 2.331 eV) and 355 nm photons ($h\nu$ = 3.493 eV). In the 532 nm spectrum of $[TaO_3]^-$, the photoelectron intensity rapidly decreased at the high electron binding energy end (>1.95 eV). Since such a decrease around 1.95 eV was not observed in the 355 nm spectrum, this decrease in the 532 nm spectrum was attributed to the limited transmission of the low kinetic energy electrons (EKE < 0.38 eV) through the magnetic bottle electron energy analyzer. The same behavior was observed in the 532 nm spectra of $[TaO_3CD_n]^-$ (n = 0, 2, 4) as well. On the other hand, the photoelectron intensity in the 355 nm spectrum of $[TaO_3]^-$ starts decreasing at EBE = 3.04 eV. The corresponding electron kinetic energy (0.46 eV) is higher than EKE = 0.38 eV, where the electron transmission efficiency started to drop in the 532 nm spectrum. Therefore, the 3.04 eV feature in the 355 nm spectrum of $[TaO_3]^-$ is a real photoelectron peak, not an artificial feature originating from the characteristic of the electron energy analyzer. The broad feature with a peak around 3.0 eV is consistent with the 355 nm aPES in a previous publication.[41]

The aPES of the methane adduct, $[TaO_3CD_4]^-$, showed a peak similar to $[TaO_3]^-$ at 3.06 eV (EKE = 0.44 eV). In addition, it showed new peaks around 1.30 eV and 1.85 eV in both 532 nm and 355 nm spectrum, and a broad feature around 2.6 eV in the 355 nm spectrum. These aPES tell whether $[TaO_3CD_4]^-$ is a physisorption complex $[TaO_3]^-(CD_4)$, where $[TaO_3]^-$ is solvated by intact CD_4, or a chemisorption complex, where the C–D bond of CD_4 is activated by $[TaO_3]^-$. In the case of a physisorption complex, it is well-known that the solvated anion remains the chromophore and the overall spectral profile does not change.[52] While the solvation effect could shift the entire electron binding energy, the shift amount is small in case of physisorption by the nonpolar and weakly polarizable methane molecule.[43] On the other hand, in the case of a chemisorption complex, the anion causes a chemical reaction with the molecule, and the resultant complex has a different

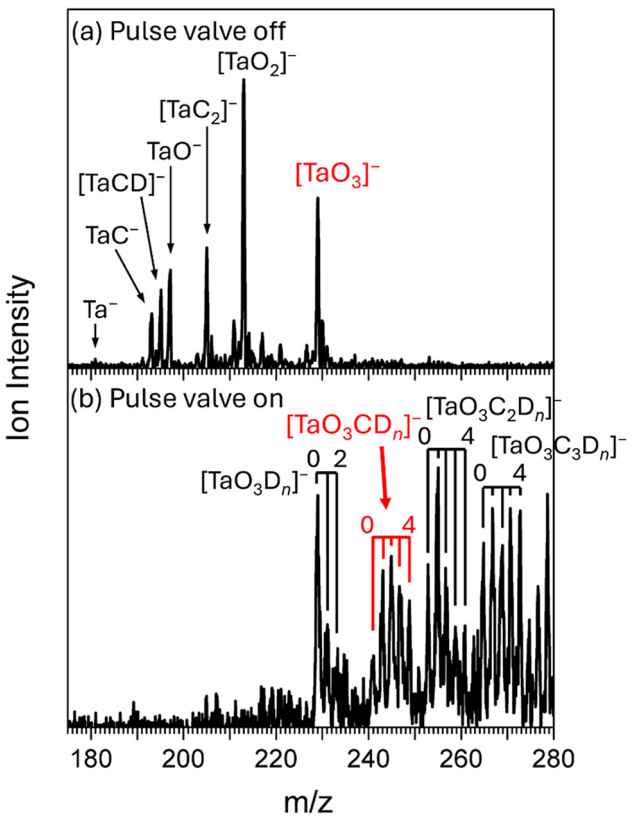

Fig. 1 Mass spectra obtained by laser vaporization of a tantalum foil with the pulse valve (CD_4/He gas mixture) off (a) and on (b).

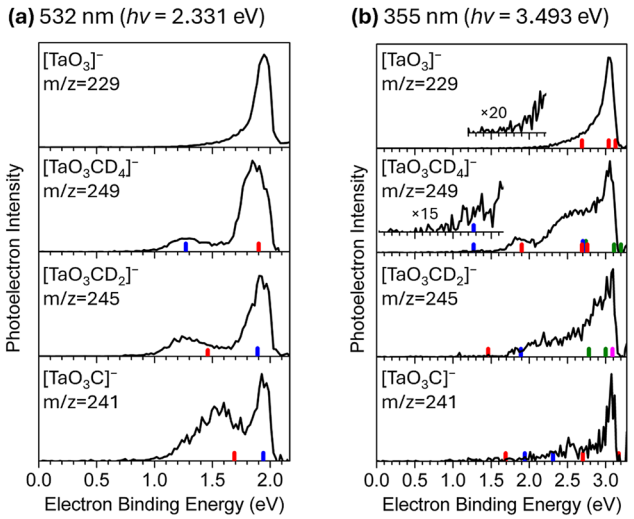

Fig. 2 Anion photoelectron spectra (aPES) of $[TaO_3]^-$ and $[TaO_3CD_n]^-$ (n = 0, 2, 4) recorded with 532 nm photons (a) and 355 nm photons (b). The stick spectra show the calculated electron binding energies. For $[TaO_3]^-$, the red sticks correspond to Fig. 4(c). For $[TaO_3CD_4]^-$, the red, blue, and green sticks correspond to the one C–H bond-cleaved chemisorption complex in Fig. 6(d), the two C–H bonds-cleaved chemisorption complex in Fig. 7, and the physisorption complex in Fig. 5(d), respectively. For $[TaO_3CD_2]^-$, the red, blue, green, and purple sticks correspond to isomers (a), (b), (c), and (d) in Fig. S1, respectively. For $[TaO_3C]^-$, the red and blue sticks correspond to isomers (a) and (b) in Fig. S2, respectively.

electronic structure from the original anion. Therefore, the aPES of the chemisorption complex shows different features from the original anion.[43,53,54] Based on this knowledge, the 3.06 eV peak of $[TaO_3CD_4]^-$ was attributed to the physisorption complex, $[TaO_3]^-(CD_4)$, and the new features around 1.30 eV, 1.85 eV, and 2.6 eV were attributed to the chemisorption complex(es). The geometrical structure of each complex is identified by comparison to the DFT calculation results in the following section.

The 355 nm aPES of all the $[TaO_3CD_n]^-$ (n = 0, 2, 4) and $[TaO_3]^-$ anions showed a peak around 3.0 eV. It indicates that this feature originates from the $[TaO_3]^-$ core common to these anions.

3.2. Computational results

As outlined in Section 2.2, the global and local minima structures of $[TaO_3]^-$ cluster were predicted by integrating the ABCluster[47,48] package with Gaussian16,[49] which was utilized for geometry optimization and energy evaluation. To account for the dependence of the optimization results on the choice of DFT functional and basis set, the minima searches were carried out at two different levels of theory, namely, B3LYP/def2-SVP and PBE0/SDD. Interestingly, our calculations in both levels of theory showed consistent results and revealed three possible $[TaO_3]^-$ minima as shown in Fig. 3. To further increase the accuracy of the energy and geometry calculations, these three isomers (A, B, and C) were further optimized using B3LYP/def2-QZVPD level. A reasonable range of spin multiplicity (S) of 1 to 5 was also investigated during the optimization to ensure proper inclusion of spin polarization on the calculated geometries and energies. It is noted that the energies of the three isomers with S = 5 are higher compared to S = 1 or 3 geometries. Moreover, for all three isomers, significant convergence difficulties and/or cluster dissociation are observed at $S \geq 5$. Consequently, only singlet and triplet spin states are considered in the present study. DFT calculation reveals that the ground states of all three local minima are singlet and the global minimum (B3LYP/def2-QZVPD) for $[TaO_3]^-$ is identified as a trigonal pyramidal structure (iso-A in Fig. 3) of C_{3v} symmetry. This is consistent with the computational results by He *et al.*[38] The triplet state of iso-A is ~1.5 eV higher compared to the singlet ground state. The relative energy ordering of the three isomers in both singlet and triplet states is provided in Table S1 in the SI. Energetically, iso-B (singlet, point group C_s) is observed to be 4.0 eV higher in energy compared to the global minimum (*i.e.*, iso-A). In iso-B, the core Ta atom is coordinated to one terminal oxygen and to an η^2-peroxo $[O_2^{2-}]$ ligand (Fig. 3). The triplet isomer of iso-B is 0.19 eV higher compared to the singlet ground state. As shown in Fig. 3, the third calculated isomer, iso-C, exhibits C_s symmetry. In this structure, the central Ta atom is bonded to a terminal oxygen atom and coordinated to an η^1-superoxo $[O_2^-]$ ligand in an end-on configuration. Notably, the singlet geometry of iso-C is nearly 5.1 eV higher compared to the global minimum, *i.e.*, the singlet geometry of iso-A. The triplet state of iso-C is 0.7 eV higher in energy compared to the singlet state.

Fig. 4 shows the simulated anion photoelectron spectra (aPES) for the singlet states of all three isomers of $[TaO_3]^-$. As shown in Fig. 4(a), the calculated vertical detachment energy (VDE) of iso-A, which is the most stable structure, is 4.46 eV. This is beyond our experimental energy range of $h\nu$ = 3.49 eV

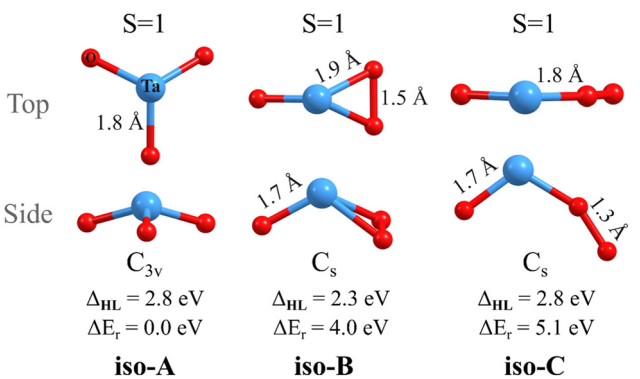

Fig. 3 Top and side views of the optimized geometries for three predicted isomers of $[TaO_3]^-$ (iso-A, iso-B, and iso-C) obtained by B3LYP/def2-QZVPD level of theory. Bond lengths are shown in Å. The point group symmetries, HOMO–LUMO gaps, and relative energies (w.r.t. iso-A) are also indicated. Ta atoms are shown in blue, and O atoms are shown in red.

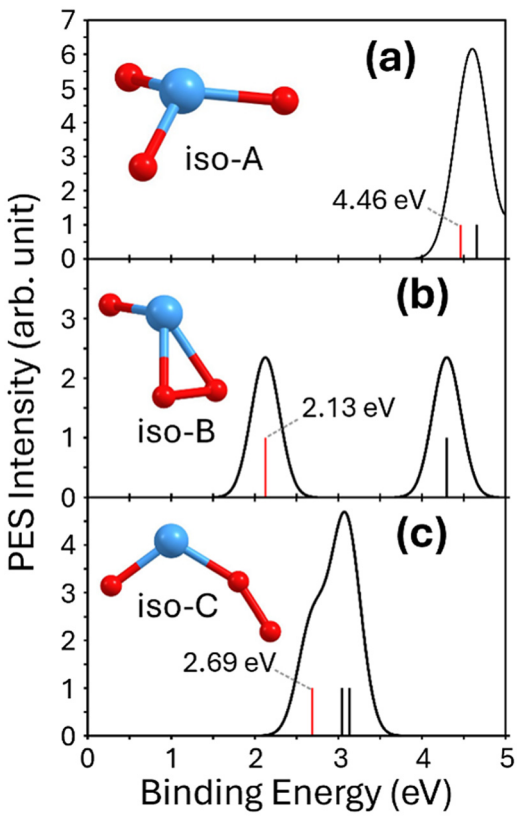

Fig. 4 Simulated anion photoelectron spectra (aPES) of the three isomers of $[TaO_3]^-$. For each isomer, the vertical detachment energy (VDE) from the anionic ground state to the neutral ground state is shown in eV and presented by the red stick. The black sticks represent the transitions from the ground state anion to the electronic excited states of the neutral. The geometrical structure of each isomer optimized by B3LYP/def2-QZVPD level of theory is shown.

(355 nm). Therefore, even if iso-A exists in our $[TaO_3]^-$ ion beam, it will not appear in our experimental spectrum. The other two isomers correspond to structures with the O–O bond intact. While the calculated VDE of iso-B is 2.13 eV, no peak was observed around this energy in the experimental spectrum (Fig. 2(b)). On the other hand, the calculated VDE of iso-C is 2.69 eV, and the predicted photoelectron feature obtained by convolving the broadened stick spectra starts from ~2.0 eV and peaks around 3.0 eV. This is consistent with the experimentally observed spectral feature of $[TaO_3]^-$. Further evidence for the existence of iso-C will be provided by comparison of the experimental and computational results of $[TaO_3CD_4]^-$ physisorption and chemisorption complexes. The existence of less stable iso-C, whose O–O bond is intact, under the present experimental conditions is related to the high bond dissociation energy of $D_0(O_2)$ = 493.69 kJ mol^{-1}.[1]

The calculated geometries and the simulated aPES of the $[TaO_3(CH_4)]^-$ complex are shown in Fig. 5. Similar to $[TaO_3]^-$, the lowest energy structures obtained for all $[TaO_3(CH_4)]^-$ isomers are singlet. The relative energy ordering is provided in Table S2 in the SI. For all three isomers, the methane molecule showed physisorption with the $[TaO_3]^-$ cluster anion. It can be seen by comparing Fig. 5 to Fig. 4 that physisorption of CH_4 onto $[TaO_3]^-$ causes shifts of the computed VDEs, while the predicted spectral profiles are preserved. In case of iso-A, we have included two different configurations, *i.e.*, iso-A(i) and iso-A(ii). Iso-A(i) is the global minimum and iso-A(ii) is nearly 0.25 eV higher compared to iso-A(i). Iso-A(i) and (ii) showed VDEs of 4.20 eV and 4.56 eV, and they are out of our experimental spectral energy range. The VDEs of iso-B and iso-C are shifted to 2.20 eV and 2.74 eV, respectively. The peak at 3.06 eV in the experimental aPES of $[TaO_3CD_4]^-$ (Fig. 2(b)) is attributed to the physisorption complex of iso-C (Fig. 5(d)).

To assign the experimental aPES features around 1.30 eV, 1.85 eV, and 2.6 eV (Fig. 2), we have performed geometry optimizations of $[TaO_3CH_4]^-$ chemisorption complexes in which one and two C–H bonds of methane are dissociated. For one C–H bond-cleaved complex, calculations were performed for the ground state (singlet) of all four isomer geometries as predicted in Fig. 5(a)–(d). The resulting lowest energy structures along with the simulated aPES are depicted in Fig. 6. For iso-A(i) and (ii), the computed VDEs are out of our experimental energy range and will not appear in our experimental aPES. While iso-B has a calculated VDE of 1.50 eV, this feature was not observed in the experimental aPES. On the other hand, the simulated aPES of iso-C has a VDE peak at 1.90 eV and a convolved peak around 2.7 eV (Fig. 6(d)). The 1.85 eV and 2.6 eV features in the experimental aPES agree with these simulated peaks, thus they were assigned to iso-C chemisorption complex. Next, consider the optimized structure and the simulated aPES of two C–H bonds-cleaved complex presented in Fig. 7. In this structure, one H atom of iso-C in Fig. 6 has migrated from the carbon atom to the O_2 ligand. The two predicted peaks of 1.27 eV and 2.70 eV agree well with the 1.30 eV and 2.6 eV features in the experimental aPES in Fig. 2. Therefore, the structures of the $[TaO_3CH_4]^-$ chemisorption complexes observed in the experimental aPES were determined to be one C–H bond-cleaved isomer (iso-C in Fig. 6) and two C–H bonds-cleaved isomer (Fig. 7).

Geometry optimizations were performed for $[TaO_3CH_2]^-$ and $[TaO_3C]^-$ clusters too, and their simulated aPES are presented in Fig. S1 and S2 in the SI, respectively. The computed spectra of both clusters reveal that the experimental aPES features most likely originated from multiple isomeric contributions. For $[TaO_3CH_2]^-$, four isomers were identified (Fig. S1). Isomer (a), characterized by a dissociated H atom and a bridging CH group bonded to the O and Ta atoms, exhibits a VDE of 1.46 eV, which is close to the 1.24 eV feature in the experimental aPES. Isomer (b), in which a bridging CH_2 group is bonded to the O and Ta atoms, yields a VDE of 1.89 eV, in excellent agreement with the 1.91 eV feature in the experimental aPES. Isomers (c) and (d),

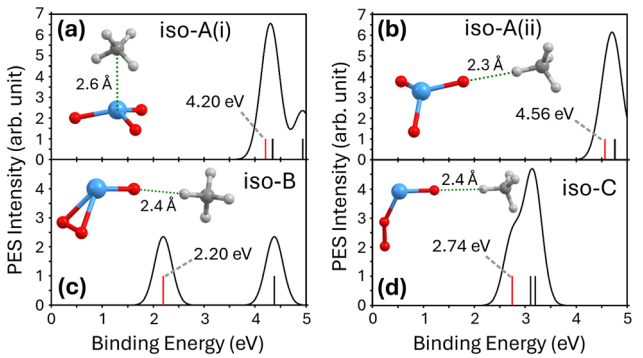

Fig. 5 Simulated anion photoelectron spectra (aPES) of the $[TaO_3(CH_4)]^-$ physisorption complexes in four geometries, (a)–(d). For each isomer, the vertical detachment energy (VDE) from the anionic ground state to the neutral ground state is shown in eV and presented by the red stick. The black sticks represent the transitions from the ground state anion to the electronic excited states of the neutral. The geometrical structure of each isomer optimized by B3LYP/def2-QZVPD level of theory is shown, with the bond length in Å.

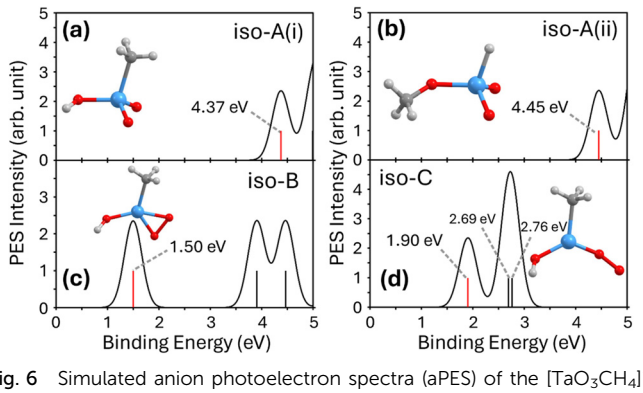

Fig. 6 Simulated anion photoelectron spectra (aPES) of the $[TaO_3CH_4]^-$ chemisorption complexes in four geometries, (a)–(d), in which one C–H bond of methane was cleaved. For each isomer, the vertical detachment energy (VDE) from the anionic ground state to the neutral ground state is shown in eV and presented by the red stick. The black sticks represent the transitions from the ground state anion to the electronic excited states of the neutral. The geometrical structure of each isomer optimized by B3LYP/def2-QZVPD level of theory is shown. Compare the simulated spectrum of iso-C to the experimental spectrum of $[TaO_3CD_4]^-$ in Fig. 2.

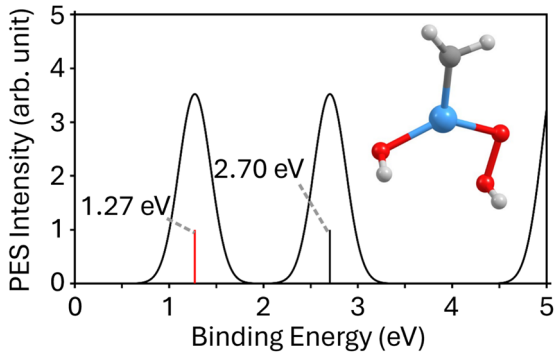

Fig. 7 Simulated anion photoelectron spectrum (aPES) of the $[TaO_3CH_4]^-$ chemisorption complex in which two C–H bonds of methane were cleaved. The vertical detachment energy (VDE) from the anionic ground state to the neutral ground state is shown in eV and presented by the red stick. The black stick represents the transition from the ground state anion to the electronic excited state of the neutral. The geometrical structure optimized by B3LYP/def2-QZVPD level of theory is shown. Compare this simulated spectrum to the experimental spectrum of $[TaO_3CD_4]^-$ in Fig. 2.

where the CH_2 group is directly attached to the central Ta atom, display transitions that correspond to the experimental aPES feature around 3 eV. Collectively, these results demonstrate that the experimental aPES of $[TaO_3CD_2]^-$ is a cumulative manifestation of multiple isomeric contributions, rather than originating from a single cluster structure. Similarly, the simulated aPES of two structurally distinct $[TaO_3C]^-$ isomers are presented in Fig. S2. The first isomer (a), where the carbon atom is bonded exclusively to one of the oxygen atoms, shows a VDE of 1.69 eV, accompanied by the second feature appearing around 2.7–3.2 eV. These resemble the 1.60 eV and ~3 eV features in the experimental aPES. The second isomer (b) is characterized by the carbon atom coordinated to both O and Ta atoms. The simulated aPES of this structure yields a VDE of 1.94 eV, corresponding to the experimental feature observed at 1.93 eV.

The experimental aPES of the bare $[TaO_3]^-$ and its methane adduct, $[TaO_3CD_4]^-$, consistently showed features originating from the $[TaO_3]^-$ in the iso-C structure and its physisorption/chemisorption complexes. While the more stable iso-A species of all the bare $[TaO_3]^-$ and the physisorption/chemisorption complexes could not be observed by the experimental spectra due to the photon energy limit, their most stable geometrical structures obtained by DFT calculations in the present study (iso-A(i) for physisorption/chemisorption complexes) were consistent with those obtained by He *et al.*'s calculations.[38]

4. Conclusions

In summary, the reactivity of $[TaO_3]^-$ toward a methane molecule was investigated by anion photoelectron spectroscopy and DFT calculations. While the computational results of the most stable trigonal pyramidal isomer of $[TaO_3]^-$ and its physisorption/chemisorption complexes with methane were consistent with the previous publication,[38] their existence could not be experimentally confirmed due to the predicted high electron binding energies of these anions beyond our experimental energy range. A particular isomer of $[TaO_3]^-$, where the Ta atom is bonded to a terminal O atom and an η^1-superoxo $[O_2^-]$ ligand, was identified computationally and observed in the experimental spectrum. Combination of anion photoelectron spectroscopy and DFT calculations showed that this isomer forms two types of activation complexes with methane by cleaving one and two C–H bonds, as well as a physisorption complex, and their geometrical structures were determined. The results obtained in the present study on the unique reactivity of $[TaO_3]^-$ toward methane are complementary to the previous works by He *et al.*, and provide the first direct spectroscopic evidence of the C–H bond activation by tantalum oxide anions, which had only been predicted theoretically prior to this work.

Author contributions

Tatsuya Chiba (investigation, writing – original draft), Turbasu Sengupta (investigation, writing – original draft), Shiying Wang (investigation), Martin Tschurl (investigation), Ulrich Heiz (investigation), Shiv N. Khanna (investigation, writing – review & editing, supervision, project administration, funding acquisition, resources), Kit H. Bowen (investigation, writing – review & editing, supervision, project administration, funding acquisition, resources).

Conflicts of interest

There are no conflicts to declare.

Data availability

The data that support the findings of this study are available in the manuscript and the supplementary information (SI). Supplementary information: Simulated anion photoelectron spectra of $[TaO_3CH_2]^-$ (Fig. S1); Simulated anion photoelectron spectra of $[TaO_3C]^-$ (Fig. S2); Relative energy ordering of the computationally predicted $[TaO_3]^-$ isomers (Table S1); Relative energy ordering of the computationally predicted $[TaO_3(CH_4)]^-$ isomers (Table S2). See DOI: https://doi.org/10.1039/d6cp01899h.

Acknowledgements

The experimental material in this work is based on support from the Air Force Office of Scientific Research (AFOSR) under grant number FA9550-22-1-0271 (K. H. B.). TS and SNK gratefully acknowledge funding by the United States Air Force Office of Scientific Research (AFOSR).

References

1 B. Ruscic and D. H. Bross, *Active Thermochemical Tables (ATcT) values based on ver. 1.220 of the Thermochemi-*

cal Network, Argonne National Laboratory, Lemont, Illinois, USA, 2025. https://atct.anl.gov/Thermochemical%20Data/version%201.220/index.php (accessed 2025-10-01).
2 H. Rodhe, A Comparison of the Contribution of Various Gases to the Greenhouse Effect, *Science*, 1990, **248**, 1217–1219, DOI: 10.1126/science.248.4960.1217.
3 D. Schröder and H. Schwarz, $FeO^{\oplus}$ Activates Methane, *Angew. Chem., Int. Ed. Engl.*, 1990, **29**, 1433–1434, DOI: 10.1002/anie.199014331.
4 H. Schwarz, Activation of Methane, *Angew. Chem., Int. Ed. Engl.*, 1991, **30**, 820–821, DOI: 10.1002/anie.199108201.
5 D. Schröder and H. Schwarz, Gas-phase activation of methane by ligated transition-metal cations, *Proc. Natl. Acad. Sci. U. S. A.*, 2008, **105**, 18114–18119, DOI: 10.1073/pnas.0801849105.
6 E. E. Claveau, S. Sader, B. A. Jackson, S. N. Khan and E. Miliordos, Transition metal oxide complexes as molecular catalysts for selective methane to methanol transformation: any prospects or time to retire?, *Phys. Chem. Chem. Phys.*, 2023, **25**, 5313–5326, DOI: 10.1039/D2CP05480A.
7 D. H. R. Barton, The Invention of Chemical Reactions, *Aldrichim. Acta*, 1990, **23**, 3–10.
8 C. Copeŕet, C–H Bond Activation and Organometallic Intermediates on Isolated Metal Centers on Oxide Surfaces, *Chem. Rev.*, 2010, **110**, 656–680, DOI: 10.1021/cr900122p.
9 K. K. Irikura and J. L. Beauchamp, Osmium Tetroxide and Its Fragment Ions in the Gas Phase: Reactivity with Hydrocarbons and Small Molecules, *J. Am. Chem. Soc.*, 1989, **111**, 75–85, DOI: 10.1021/ja00183a014.
10 S. W. Buckner, T. J. MacMahon, G. D. Byrd and B. S. Freiser, Gas-Phase Reactions of Nb^+ and Ta^+ with Alkanes and Alkenes. C–H Bond Activation and Ligand-Coupling Mechanisms, *Inorg. Chem.*, 1989, **28**, 3511–3518, DOI: 10.1021/ic00317a024.
11 K. L. Irikura and J. L. Beauchamp, Methane Oligomerization in the Gas Phase by Third-Row Transition-Metal Ions, *J. Am. Chem. Soc.*, 1991, **113**, 2769–2770, DOI: 10.1021/ja00007a070.
12 K. K. Irikura and J. L. Beauchamp, Electronic Structure Considerations for Methane Activation by Third-Row Transition-Metal Ions, *J. Phys. Chem.*, 1991, **95**, 8344–8351, DOI: 10.1021/j100174a057.
13 R. Wesendrup and H. Schwarz, Tantalum-Mediated Coupling of Methane and Carbon Dioxide in the Gas Phase, *Angew. Chem., Int. Ed. Engl.*, 1995, **34**, 2033–2035, DOI: 10.1002/anie.199520331.
14 N. Sändig and W. A. Koch, Quantum Chemical View on the Mechanism of the Ta^+-Mediated Coupling of Carbon Dioxide with Methane, *Organometallics*, 1998, **17**, 2344–2351, DOI: 10.1021/om971141l.
15 L. G. Parke, C. S. Hinton and P. B. Armentrout, Experimental and Theoretical Studies of the Activation of Methane by Ta^+, *J. Phys. Chem. C*, 2007, **111**, 17773–17787, DOI: 10.1021/jp070855z.
16 A. Shayesteh, V. V. Lavrow, G. K. Koyanagi and D. K. Bohme, Reactions of Atomic Cations with Methane: Gas Phase Room-Temperature Kinetics and Periodicities in Reactivity, *J. Phys. Chem. A*, 2009, **113**, 5602–5611, DOI: 10.1021/jp900671c.
17 V. J. F. Lapoutre, B. Redlich, A. F. G. van der Meer, J. Oomens, J. M. Bakker, A. Sweeney, A. Mookherjee and P. B. Armentrout, Structures of the Dehydrogenation Products of Methane Activation by 5d Transition Metal Cations, *J. Phys. Chem. A*, 2013, **117**, 4115–4126, DOI: 10.1021/jp400305k.
18 P. B. Armentrout, Methane Activation by 5d Transition Metals: Energetics, Mechanisms, and Periodic Trends, *Chem. – Eur. J.*, 2017, **23**, 10–18, DOI: 10.1002/chem.201602015.
19 J. F. Eckhard, T. Masubuchi, M. Tschurl, R. N. Barnett, U. Landman and U. Heiz, Thermal Dehydrogenation of Methane Enhanced by μ_2-Oxo Ligands in Tantalum Cluster Cations $[Ta_xO]^+$, x = 4, 5, *J. Phys. Chem. C*, 2018, **122**, 25628–25637, DOI: 10.1021/acs.jpcc.8b07729.
20 J. Lengyel, N. Levin, F. J. Wensink, O. V. Lushchikova, R. N. Barnett, U. Landman, U. Heiz, J. M. Bakker and M. Tschurl, Carbide Dihydrides: Carbonaceous Species Identified in Ta_4^+-Mediated Methane Dehydrogenation, *Angew. Chem., Int. Ed.*, 2020, **59**, 23631–23635, DOI: 10.1002/anie.202010794.
21 J. F. Eckhard, T. Masubuchi, M. Tschurl, R. N. Barnett, U. Landman and U. Heiz, Room-Temperature Methane Activation Mediated by Free Tantalum Cluster Cations: Size-by-Size Reactivity, *J. Phys. Chem. A*, 2021, **125**, 5289–5302, DOI: 10.1021/acs.jpca.1c02384.
22 J. Lengyel, N. Levin, M. Ončák, K. Jakob, M. Tschurl and U. Heiz, Direct Coupling of Methane and Carbon Dioxide on Tantalum Cluster Cations, *Chem. – Eur. J.*, 2023, **29**, e202203259, DOI: 10.1002/chem.202203259.
23 F. Siegele, M. Tschurl, D. Schooss and U. Heiz, Activation of CH_4, NH_3, and N_2 by Tantalum Ions, Clusters and Their Oxides: What Can Be Learnt from Studies of Ions in the Gas Phase, *ChemPhysChem*, 2025, **26**, e202400513, DOI: 10.1002/cphc.202400513.
24 Y. Xu, Z.-Y. Li, Q. Yang, X.-G. Zhao, Q. Li and S.-G. He, Machine Learning Study of Methane Activation by Gas-Phase Species, *J. Phys. Chem. A*, 2025, **129**, 1941–1951, DOI: 10.1021/acs.jpca.4c06602.
25 M. Firouzbakht, N. J. Rijs, P. González-Navarrete, M. Schlangen, M. Kaupp and H. Schwarz, On the Activation of Methane and Carbon Dioxide by $[HTaO]^+$ and $[TaOH]^+$ in the Gas Phase: A Mechanistic Study, *Chem. – Eur. J.*, 2016, **22**, 10581–10589, DOI: 10.1002/chem.201601339.
26 G. Wang, S. Lai, M. Chen and M. Zhou, Matrix Isolation Infrared Spectroscopic and Theoretical Studies on the Reactions of Niobium and Tantalum Mono- and Dioxides with Methane, *J. Phys. Chem. A*, 2005, **109**, 9514–9520, DOI: 10.1021/jp053666u.
27 S. Zhou, J. Li, M. Schlangen and H. Schwarz, Differences and Commonalities in the Gas-Phase Reactions of Closed-Shell Metal Dioxide Clusters $[MO_2]^+$ (M = V, Nb, and Ta) with

Mehtane, *Chem. – Eur. J.*, 2016, **22**, 7225–7228, DOI: 10.1002/chem.201600498.
28 S. Zhou, J. Li, M. Schlangen and H. Schwarz, Spin-Selective Thermal Activation of Methane by Closed-Shell $[TaO_3]^+$, *Angew. Chem., Int. Ed.*, 2016, **55**, 7257–7260, DOI: 10.1002/anie.201601965.
29 N. Levin, J. Lengyel, J. F. Eckhard, M. Tschurl and U. Heiz, Catalytic Non-Oxidative Coupling of Methane on $Ta_8O_2^+$, *J. Am. Chem. Soc.*, 2020, **142**, 5862–5869, DOI: 10.1021/jacs.0c01306.
30 Q. Liu, Q.-Y. Liu, Y.-X. Zhao and S.-G. He, Conversion of Methane at Room Temperature Mediated by the Ta–Ta σ-Bond, *J. Am. Chem. Soc.*, 2024, **4**, 1824–1832, DOI: 10.1021/jacsau.4c00032.
31 K. A. Zemski, R. C. Bell and A. W. Castleman Jr., Reactivities of tantalum oxide cluster cations with unsaturated hydrocarbons, *Int. J. Mass Spectrom.*, 1999, **184**, 119–128, DOI: 10.1016/S1387-3806(98)14276-8.
32 K. A. Zemski, R. C. Bell and A. W. Castleman Jr., Reactions of Tantalum Oxide Cluster Cations with 1-Butene, 1,3-Butadiene, and Benzene, *J. Phys. Chem. A*, 2000, **104**, 5732–5741, DOI: 10.1021/jp000051i.
33 K. A. Zemski, D. R. Justes and A. W. Castleman Jr., Reactions of Group V Transition Metal Oxide Cluster Ions with Ethane and Ethylene, *J. Phys. Chem. A*, 2001, **105**, 10237–10245, DOI: 10.1021/jp012319r.
34 K. A. Zemski, D. R. Justes, R. C. Bell and A. W. Castleman Jr., Reactions of Niobium and Tantalum Oxide Cluster Cations and Anions with *n*-Butane, *J. Phys. Chem. A*, 2001, **105**, 4410–4417, DOI: 10.1021/jp010222z.
35 J.-H. Meng, X.-J. Deng, Z.-Y. Li, S.-G. He and W.-J. Zheng, Thermal Methane Activation by $La_6O_{10}^-$ Cluster Anions, *Chem. – Eur. J.*, 2014, **20**, 5580–5583, DOI: 10.1002/chem.201400218.
36 M. Ruan, Y.-X. Zhao, M.-Q. Zhang and S.-G. He, Methane Activation by $(MoO_3)_5O^-$ Cluster Anions: The Importance of Orbital Orientation, *Chem. – Eur. J.*, 2022, **28**, e202103321, DOI: 10.1002/chem.202103321.
37 Y. Yang, B. Yang, Y.-X. Zhao, L.-X. Jiang, Z.-Y. Li, Y. Ren, H.-G. Xu, W.-J. Zheng and S.-G. He, Direct Conversion of Methane with Carbon Dioxide Mediated by $RhVO_3^-$ Cluster Anions, *Angew. Chem., Int. Ed.*, 2019, **58**, 17287–17292, DOI: 10.1002/anie.201911195.
38 Q. Li, Q.-Y. Liu, A. Zhao and S.-G. He, Reactions between $Ta_xO_y^-$ (x = 1–5, y = 0–7) cluster anions and C_1–C_3 alkanes, *J. Chem. Phys.*, 2025, **163**, 054303, DOI: 10.1063/5.0278938.
39 Q. Li, X.-X. Liu, Q.-Y. Liu and S.-G. He, Methane activation by closed-shell tantalum sulfide anions TaS_3^-, *Chin. J. Chem. Phys.*, 2024, **37**, 823–830, DOI: 10.1063/1674-0068/cjcp2407094.
40 H.-J. Zhai, B. B. Averkiev, D. Y. Zubarev, L.-S. Wang and A. I. Boldyrev, δ Aromaticity in $[Ta_3O_3]^-$, *Angew. Chem.*, 2007, **119**, 4355–4358, DOI: 10.1002/ange.200700442.
41 W. Zheng, X. Li, S. Eustis and K. Bowen, Anion Photoelectron Spectroscopy of TaO_n^- (n = 1–3), *Chem. Phys. Lett.*, 2008, **460**, 68–71, DOI: 10.1016/j.cplett.2008.06.016.
42 H.-J. Zhai, B. Wang, X. Huang and L.-S. Wang, Structural Evolution, Sequential Oxidation, and Chemical Bonding in Tritantalum Oxide Clusters: $Ta_3O_n^-$ and Ta_3O_n (n = 1–8), *J. Phys. Chem. A*, 2009, **113**, 9804–9813, DOI: 10.1021/jp905478w.
43 T. Chiba, J. A. Olaniyan, S. Wang, Y. Han, E. Miliordos and K. H. Bowen, Activation of Methane by Group 11 (Cu, Ag, Au) and Group 9 (Co, Ir) Transition Metal Atomic Anions, *J. Phys. Chem. A*, 2025, **129**(42), 9676–9683, DOI: 10.1021/acs.jpca.5c04702.
44 C. S. Feigerle, R. R. Corderman and W. C. Lineberger, Electron affinities of B, Al, Bi, and Pb, *J. Chem. Phys.*, 1981, **74**, 1513–1515, DOI: 10.1063/1.441174.
45 X. Chen and C. Ning, Accurate electron affinity of Pb and isotope shifts of binding energies of Pb^-, *J. Chem. Phys.*, 2016, **145**, 084303, DOI: 10.1063/1.4961654.
46 J. Ho, K. M. Ervin and W. C. Lineberger, Photoelectron Spectroscopy of Metal Cluster Anions: Cu_n^-, Ag_n^-, and Au_n^-, *J. Chem. Phys.*, 1990, **93**, 6987–7002, DOI: 10.1063/1.459475.
47 J. Zhang and M. Dolg, ABCluster: the artificial bee colony algorithm for cluster global optimization, *Phys. Chem. Chem. Phys.*, 2015, **17**, 24173–24181, DOI: 10.1039/C5CP04060D.
48 J. Zhang and M. Dolg, Global optimization of clusters of rigid molecules using the artificial bee colony algorithm, *Phys. Chem. Chem. Phys.*, 2016, **18**, 3003–3010, DOI: 10.1039/C5CP06313B.
49 M. J. Frisch, G. W. Trucks, H. B. Schlegel, G. E. Scuseria, M. A. Robb, J. R. Cheeseman, G. Scalmani, V. Barone, G. A. Petersson, H. Nakatsuji, X. Li, M. Caricato, A. V. Marenich, J. Bloino, B. G. Janesko, R. Gomperts, B. Mennucci, H. P. Hratchian, J. V. Ortiz, A. F. Izmaylov, J. L. Sonnenberg, Williams, F. Ding, F. Lipparini, F. Egidi, J. Goings, B. Peng, A. Petrone, T. Henderson, D. Ranasinghe, V. G. Zakrzewski, J. Gao, N. Rega, G. Zheng, W. Liang, M. Hada, M. Ehara, K. Toyota, R. Fukuda, J. Hasegawa, M. Ishida, T. Nakajima, Y. Honda, O. Kitao, H. Nakai, T. Vreven, K. Throssell, J. A. Montgomery Jr., J. E. Peralta, F. Ogliaro, M. J. Bearpark, J. J. Heyd, E. N. Brothers, K. N. Kudin, V. N. Staroverov, T. A. Keith, R. Kobayashi, J. Normand, K. Raghavachari, A. P. Rendell, J. C. Burant, S. S. Iyengar, J. Tomasi, M. Cossi, J. M. Millam, M. Klene, C. Adamo, R. Cammi, J. W. Ochterski, R. L. Martin, K. Morokuma, O. Farkas, J. B. Foresman and D. J. Fox, *Gaussian16*, 2016.
50 T. Lu and F. Chen, Multiwfn: A multifunctional wavefunction analyzer, *J. Comput. Chem.*, 2012, **33**, 580–592, DOI: 10.1002/jcc.22885.
51 T. Lu, A comprehensive electron wavefunction analysis toolbox for chemists, Multiwfn, *J. Chem. Phys.*, 2024, **161**, 082503, DOI: 10.1063/5.0216272.
52 J. V. Coe, J. T. Snodgrass, C. B. Freidhoff, K. M. McHugh and K. H. Bowen, Photoelectron spectroscopy of the negative cluster ions $NO^-(N_2O)_{n=1,2}$, *J. Chem. Phys.*, 1987, **87**, 4302–4309, DOI: 10.1063/1.452888.

53 G. Liu, Z. Zhu, S. M. Ciborowski, I. R. Ariyarathna, E. Miliordos and K. H. Bowen, Selective Activation of the C–H Bond in Methane by Single Platinum Atomic Anions, *Angew. Chem., Int. Ed.*, 2019, **58**, 7773–7777, DOI: 10.1002/anie.201903252.

54 G. Liu, I. R. Ariyarathna, S. M. Ciborowski, Z. Zhu, E. Miliordos and K. H. Bowen, Simultaneous Functionalization of Methane and Carbon Dioxide Mediate by Single Platinum Atomic Anions, *J. Am. Chem. Soc.*, 2020, **142**, 21556–21561, DOI: 10.1021/jacs.0c11112.